Thermodynamics and mechanism of metal-induced crystallization in immiscible alloy systems: Experiments and calculations on Al/a-Ge and Al/a-Si bilayers

Z. M. Wang, J. Y. Wang,* L. P. H. Jeurgens, and E. J. Mittemeijer
Max Planck Institute for Metals Research, Heisenbergstrasse 3, D-70569 Stuttgart, Germany
(Received 27 April 2007; published 25 January 2008)

The mechanism of metal-induced crystallization (MIC) in immiscible alloy systems has been explained on a unified thermodynamic basis. Interface thermodynamics has been shown to play a decisive role for the occurrence of MIC. The thermodynamic predictions agree excellently with the corresponding experimental observations obtained in this project for the Al/Ge and Al/Si layer systems, which show two distinctly different types of MIC behaviors. As a result, a model has been developed that rationalizes and predicts MIC processes in immiscible alloy systems.

DOI: 10.1103/PhysRevB.77.045424 PACS number(s): 61.43.Dq, 05.70.Np, 68.35.−p, 81.10.Jt

I. INTRODUCTION

Interfaces in materials, incorporating interphase boundaries and grain boundaries (GBs), play an important role in the occurrence of phase transformations, particularly recognizing that the dimensions of material systems have decreased greatly.[1–4] Interface-mediated phase transformations, such as solid-state amorphization in metal-metal multilayers,[5,6] superheated melting in confined thin films,[7,8] GB wetting,[9–11] and GB premelting,[11,12] have been a focal point of interest in recent years. It has often been suggested that phase transformation phenomena occurring in particular at interfaces have a kinetic origin.

In this work, an important type of interface-mediated solid-state phase transformations is considered: metal-induced crystallization (MIC). In MIC, the crystallization temperatures of, for example, amorphous Si and amorphous Ge are drastically reduced in contact with certain metals, such as Al,[13–23] Au,[24,25] Ag,[14] and Ni.[26,27] Although MIC has been extensively studied in recent years, a generally accepted understanding of the origin of this effect has not been achieved. For various metal-amorphous semiconductor couples, the MIC behaviors are quite different, and various different, qualitative models have been proposed.[13,17,21,24,27] For immiscible layer systems (for example, Al/Ge and Al/Si), mainly two types of MIC behaviors have been reported (see, in particular, Ref. 23). (i) In the early studies on c-Al/a-Ge (where "a" denotes amorphous and "c" denotes crystalline) by transmission electron microscopy (TEM), a fractal-like crystallization of the a-Ge layer was observed and interpreted to be due to the nucleation of crystalline Ge at the c-Al/a-Ge interface.[15,24] (ii) Work on the low-temperature Al-induced crystallization of a-Si showed that in this system MIC is accompanied by a layer exchange of the Al and Si layers.[16–21] That is, c-Si grows *within* the Al layer until there forms a continuous *c*-Si layer at the position of the original Al layer.

Hence, there is the need to understand the causes of such different types of MIC behaviors. It would be very useful if a universal interpretation of various MIC behaviors could be given. The current paper addresses this question both experimentally and theoretically.

Experimentally. To rule out the possible effects of strikingly different experimental conditions in different studies, a comparative experimental investigation on the MIC processes in Al/Ge and Al/Si systems under *identical* conditions was carried out here. The results will be presented and discussed in Sec. III of this paper.

Theoretically. A general theoretical model that accounts for MIC processes in immiscible alloy systems is proposed in Sec. IV, with Al/Ge and Al/Si systems as prototype systems. In metal/c-Si (or c-Ge) layer systems, a common physical mechanism involves the weakening of the covalent bonds between interfacial Si (or Ge) atoms induced by the adjacent metal solid.[28] On this basis, for example, low-temperature silicide (or germanide) phase formation at metal/Si (or Ge) interfaces has been explained.[28] Then, first, the same bond-weakening effect of the covalent bonds of a-Si or a-Ge in contact with a metal solid can play a role in the initiation of low-temperature MIC as well.[13,16–23] As a result of the bond-weakening effect, a very thin interface-adjacent layer of more or less mobile Si (or Ge) atoms is formed, which could play a decisive role in the initiation (kinetics) of phase transformations (crystallization). Second, and more importantly, it is recognized that a phase transformation occurring at an interface can be controlled largely by interface rather than bulk thermodynamics. As will be shown in this paper, both the constraint due to the limited amount of mobile interfacial Si (or Ge) atoms and interface thermodynamics govern the MIC behavior.

Several models have been developed to describe diffusion and reactions (in particular, compound formation) in thin-film systems on a thermodynamic and/or kinetic basis.[2–6,29] Recognizing gradients in chemical potentials as driving forces for diffusional transport, it has been shown in Refs. 3 and 4 that besides atom transport *across* interphase boundaries, concurrent atom transport *along* grain and interphase boundaries (and thus the film microstructure) can play an important role in the nucleation and microstructural evolution of product alloy phases in polycrystalline thin-film diffusion couples. However, these models do not take into account the role of interface (and surface) energies on the energetics of (thin-film) reactions, such that direct practical application is possible. Recently, a description of *interface* thermodynamics has been developed on the basis of the so-called macroscopic atom approach,[30,31] which has success-

 ©2008 The American Physical Society

fully predicted experimentally observed thin-film microstructures that differ strikingly from those known and predicted by *bulk* thermodynamics.[5,6,32,33] Hence, such "unexpected" microstructures can be thermodynamically (instead of kinetically) preferred because of the relatively large contributions of the interface and surface energies to the total energy of the thin-film system.[5,6,31–33] On this basis, the various types of MIC behaviors can be rationalized, as shown in this paper. The model has been successfully applied not only to the Al/Ge and Al/Si systems studied experimentally in this work, but also to the Ag/Si and Au/Si systems for which experimental MIC data have been reported previously.

II. EXPERIMENT

Four bilayer specimens, c-Al/a-Ge (i.e., with c-Al sublayer on top of a-Ge sublayer), a-Ge/c-Al, c-Al/a-Si, and a-Si/c-Al, were prepared at room temperature (RT) by sputter deposition in an ultrahigh-vacuum chamber (base pressure of 10^{-7} Pa). Si(510) wafers covered with a 50 nm thermal-grown SiO_2 layer were used as substrates. The sputter apparatus had two exchangeable targets: one mounted with Al (99.999 wt %) and the other mounted with Ge (or Si, both 99.999 wt %), which allowed the preparation of each bilayer specimen in a single run without interrupting the ultrahigh vacuum. The thickness of the as-prepared Al layer was 50 nm, and the thickness of the as-prepared a-Ge or a-Si layer was 150 nm for all four specimens.

For the *ex situ* investigations, the as-deposited specimens were cut into pieces of lateral dimensions 10×10 mm^2, enclosed in a glass capsule containing pure Ar gas and subsequently annealed at 165 and 250 °C for a certain time in a furnace. The MIC behaviors of the specimens upon *ex situ* annealing were investigated by applying x-ray diffraction (XRD), Auger electron spectroscopy (AES), and scanning electron microscopy (SEM).

The XRD measurements were carried out by using a Philips X'Pert MRD Pro diffractometer equipped with an x-ray lens and a Cu x-ray tube operating in point-focus geometry (45 kV/40 mA). The Cu $K\alpha$ radiation was selected by a flat graphite monochromator placed in the diffracted beam path. The diffractions patterns of the as-deposited and the annealed specimens were recorded by performing θ-2θ scanning (2θ: diffraction angle) under continuous mode. The SEM and AES composition mappings of the surfaces of the as-deposited and the annealed specimens were performed using a JEOL JAMP-7830F scanning Auger microscope. During the measurements, a focused 10 keV electron beam with a diameter of about 20 nm was employed. The concentration-depth profiles of the specimens were determined by employing a discontinuous Ar^+ (1 keV) sputtering mode. The sputtered and analyzed areas were 1×1 mm^2 and 10×10 μm^2, respectively.

The crystallization kinetics of a-Ge and a-Si in the Al/Ge and Al/Si layer systems were investigated by *in situ* XRD measurements. These *in situ* measurements were carried out on a Bruker D8 Discover diffractometer comprising a rotating-anode x-ray source (Bruker TXS, Cu $K\alpha$ radiation, as selected by an incident beam x-ray mirror in combination with a Bruker SolX energy-dispersive detector) and a vacuum heating and/or cooling stage (Anton Paar DCS350, calibrated as described in Ref. 34). The as-deposited c-Al/a-Ge, a-Ge/c-Al, c-Al/a-Si, and a-Si/c-Al specimens were *in situ* heated for two cycles sequentially: (a) heating up from RT to 165 °C in steps of 25 °C, and then cooling down in steps of 25 °C to RT; (b) heating up from RT to 250 °C in steps of 25 °C, and then cooling down in steps of 25 °C to RT. At each temperature step, the specimen was held for 30 min before the diffraction measurements were made; at the highest temperatures of 165 °C (first cycle) and 250 °C (second cycle), the specimens were held and measured at three accumulative annealing times: 30 min, 2 h, and 4 h.

III. EXPERIMENTAL RESULTS

A. Intermixing and crystallization upon *ex situ* annealing

1. Al/a-Ge and a-Ge/Al

The compositional concentration-depth profiles of the Al/a-Ge specimen upon *ex situ* annealing at various temperatures and times are shown in Fig. 1(a). For the as-deposited Al/a-Ge specimen, a sharp interface between Al and Ge is observed (for a quantitative discussion of the instrumental smearing effects, see Ref. 35). After annealing at 165 °C for 10 min, intermixing of Al and Ge has occurred. Further annealing at 165 °C for 1 day results in a further, modest change of the depth profile. Annealing at 250 °C results in much more pronounced intermixing of Al and Ge: The Al and Ge sublayers have practically exchanged their positions after annealing at 250 °C for only 10 min. Only a minor change of the depth profile occurs upon further annealing at 250 °C for 1 day.

The corresponding crystallization process of a-Ge in the Al/a-Ge specimen upon *ex situ* annealing was investigated by XRD [see the diffraction scans shown in Fig. 1(b)]. The XRD patterns shown in the figure have been processed by subtracting the XRD background recorded separately from a clean 50 nm SiO_2/Si(510) substrate. Before annealing, a very broad scattering peak at 2θ of $\sim27°$ is observed, indicating the amorphous structure of the Ge layer in the Al/a-Ge specimen. After annealing at 165 °C for 10 min, the a-Ge layer has crystallized substantially. A very strong Ge(111) peak can be observed at $2\theta\sim27.2°$. Other Ge crystalline peaks, such as Ge(220) at $\sim45.3°$ and Ge(311) at $\sim53.6°$, can also be clearly observed in the XRD pattern. Further annealing of the same sample for 1 day at 165 °C makes no difference for the XRD pattern (not shown here). At the higher annealing temperature of 250 °C, the intensities of Ge diffraction peaks, as observed after 10 min, remain constant even after annealing at 250 °C for 1 day. It is concluded that the whole a-Ge layer has fully crystallized after annealing at 165 °C for only 10 min and that no significant change of the preferred orientation (texture) occurs after a completed crystallization. At the same time, the corresponding concentration-depth profile for annealing at 165 °C, shown in Fig. 1(a), is far from indicating a layer exchange of Al and Ge layers as observed at 250 °C after 10 min annealing.

The intermixing and crystallization behaviors of the oppositely stacked a-Ge/Al specimen at the same annealing

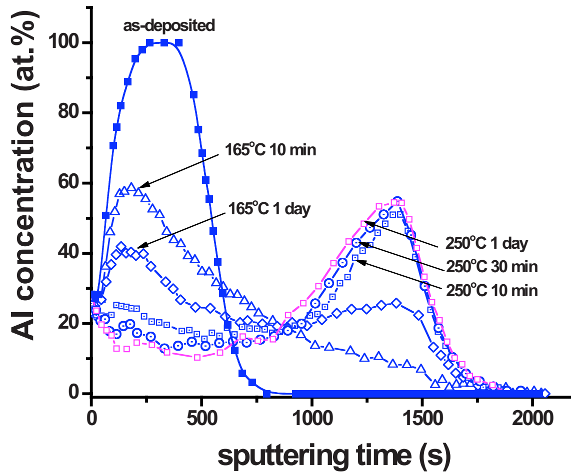

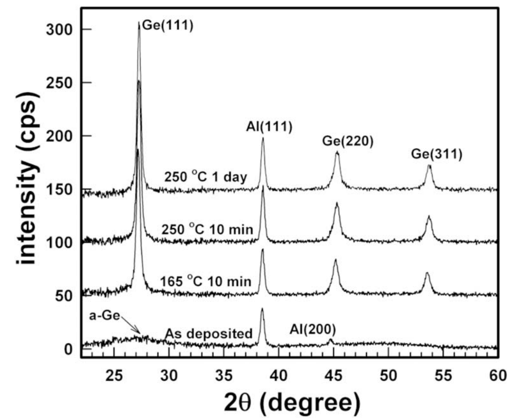

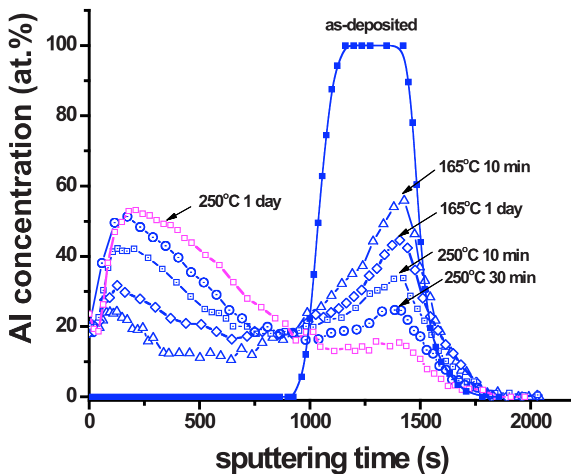

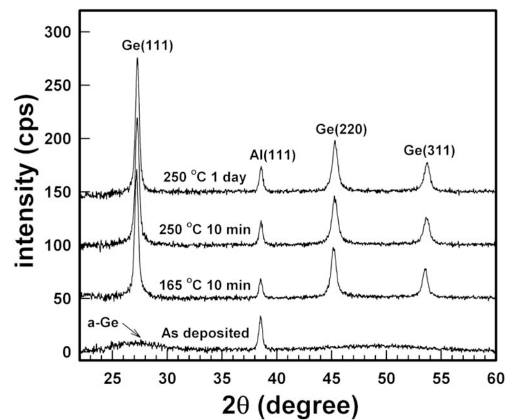

FIG. 1. (Color online) AES concentration-depth profiles of the (a) Al/a-Ge and (c) a-Ge/Al specimens upon annealing for temperatures and times as indicated. Corresponding XRD patterns are shown in (b) and (d) for Al/a-Ge and a-Ge/Al, respectively.

temperatures and times are shown in Figs. 1(c) and 1(d), respectively. A sharp interface between the a-Ge and Al sublayers is also observed for the as-deposited a-Ge/Al specimen [Fig. 1(c)]. At 165 °C, the intermixing behavior of the a-Ge/Al specimen is similar to that of the Al/a-Ge specimen. At 250 °C, however, the intermixing process is significantly slower than that in the Al/a-Ge specimen. The depth profile shows a distinctively double-peaked structure after 10 min of annealing at 250 °C. Only after annealing at 250 °C for 1 day, layer exchange of the Al and Ge sublayers has been realized.

As shown in Fig. 1(d), the a-Ge phase in the a-Ge/Al specimen shows the same crystallization behavior as that in the Al/a-Ge specimen upon annealing. The whole a-Ge layer has fully crystallized after annealing at 165 °C for only 10 min, at a stage far from layer exchange. Further intermixing of Ge and Al (layer exchange) is clearly observed upon further annealing and at higher temperatures, i.e., after a completed crystallization of the Ge phase.

2. Al/a-Si and a-Si/Al

The intermixing process in the Al/a-Si and a-Si/Al specimens under similar annealing conditions was also investigated through AES concentration-depth profile measurements [see results in Figs. 2(a) and 2(c), respectively]. At 165 and 250 °C, intermixing of Si and Al occurs in both Al/a-Si and a-Si/Al. There is a pronounced difference in the intermixing rates of Al/a-Si and a-Si/Al. In contrast with the results shown above for the Al/Ge layer systems, the intermixing is much faster if the a-Si sublayer is on the top of the specimen. At 250 °C, it takes only 1 h for a-Si/Al and a much longer time of 25 h for Al/a-Si to achieve layer exchange.

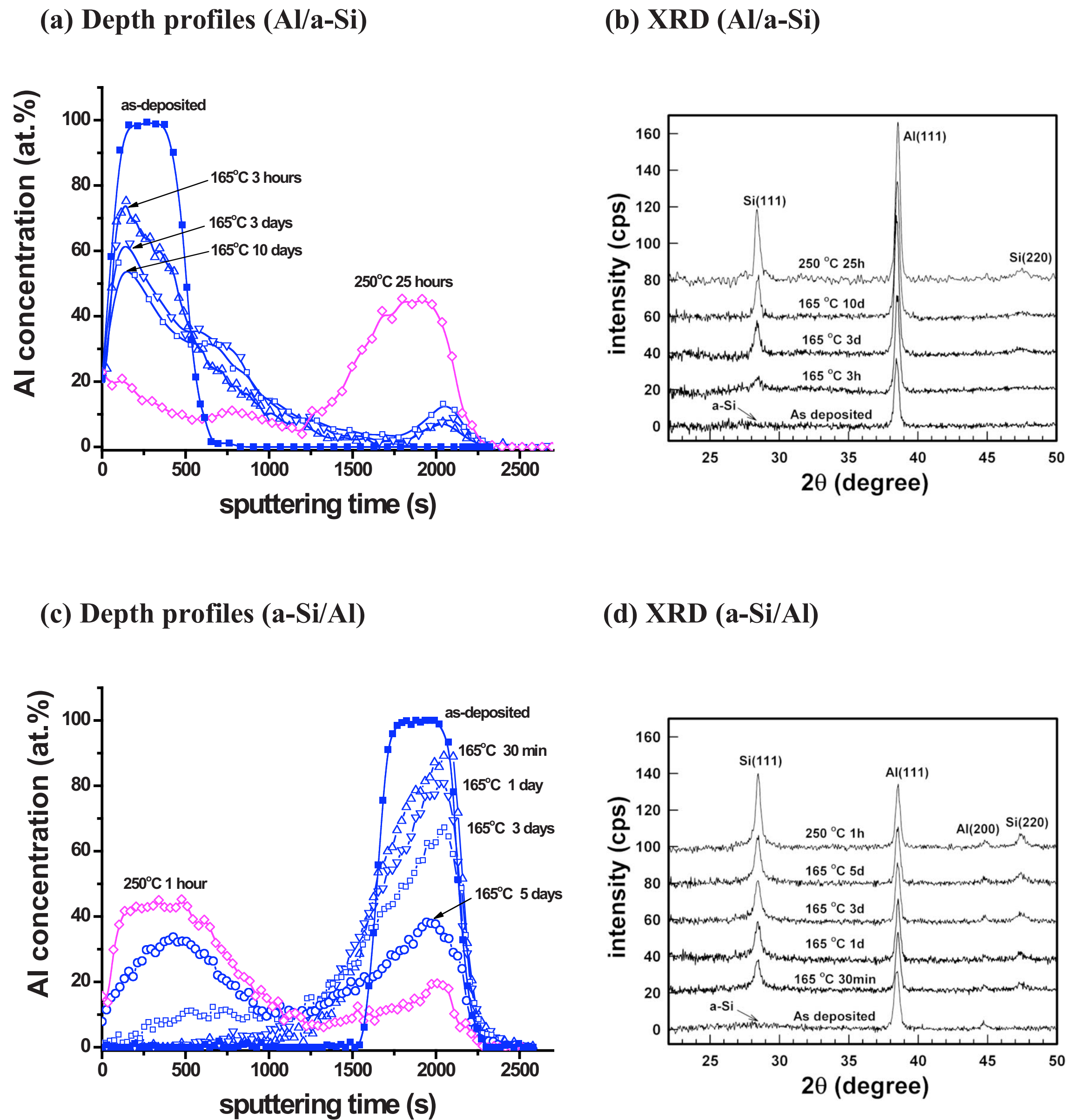

FIG. 2. (Color online) AES concentration-depth profiles of the (a) Al/a-Si and (c) a-Si/Al specimens upon annealing for temperatures and times as indicated. Corresponding XRD patterns are shown in (b) and (d) for Al/a-Si and a-Si/Al, respectively.

The crystallization of the a-Si phases during annealing of the Al/a-Si and a-Si/Al specimens was monitored through XRD measurements; results are shown in Figs. 2(b) and 2(d), respectively. For Al/a-Si and a-Si/Al, the crystallization and intermixing processes appear correlated, in contrast with the results shown above for the Al/Ge layer system. Initial crystallization of a-Si is observed at 165 °C for both specimens. Upon continued annealing, the a-Si phase becomes crystallized gradually. The a-Si phase has not fully crystallized until layer exchange of the Al and Si layers has been realized. In correspondence with the substantial difference in the intermixing rates of Al/a-Si and a-Si/Al, the a-Si phase in the a-Si/Al specimen exhibits a higher crystallization rate than that in the Al/a-Si specimen.

B. Surface morphology

The surface morphology of the Al/a-Ge specimen annealed at 165 °C for 10 min is shown in the SEM micrograph presented as Fig. 3(a). The corresponding XRD measurement has indicated that the a-Ge phase in the specimen has *fully* crystallized [Fig. 1(b)]. The micrograph shows equiaxed black areas (size: tens of nanometers) separated by branchlike white structures. Small-area (point size: 20 nm) AES analyses shown in Fig. 3(b) indicate that the black areas are Al rich while the white branches are Ge rich. The morphology shown in Fig. 3(a) remains essentially the same upon continued sputtering until reaching the original interface between the Al and Ge sublayers, which suggests that the equiaxed black areas are the columnar Al grains and the white branches are c-Ge formed between the adjacent Al

(a) Al/a-Ge 165 °C, 10 min **(b)**

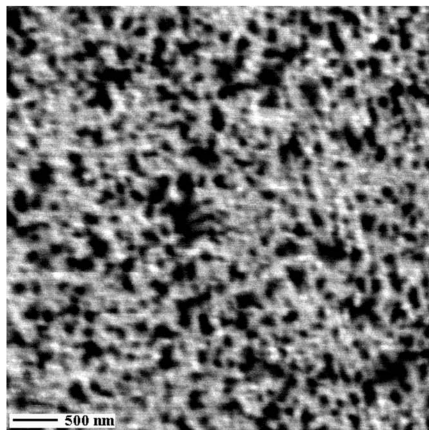

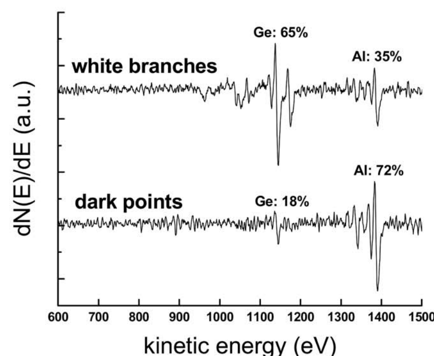

(c) a-Ge/Al 165 °C, 10 min **(d)**

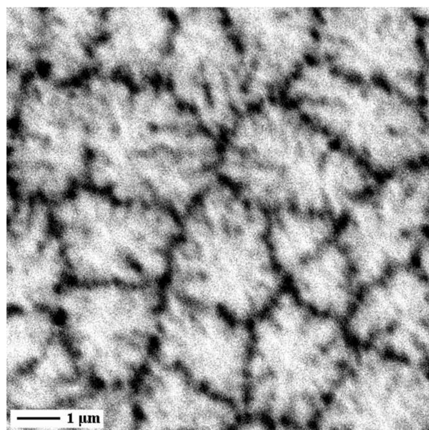

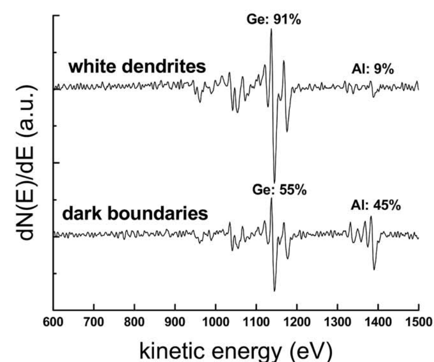

(e) a-Si/Al 165 °C, 3 days **(f)**

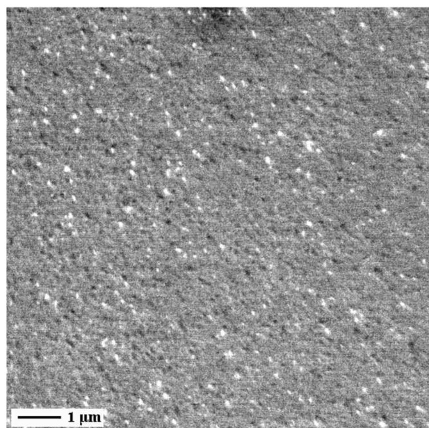

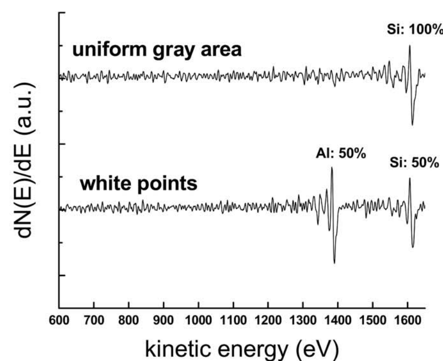

FIG. 3. SEM micrographs (recorded in the Auger microscope) of the surfaces of the (a) Al/a-Ge, (c) a-Ge/Al, and (e) a-Si/Al specimens annealed for temperatures and times as indicated. The corresponding AES analyses (derivative spectra) of small areas (size: 20 nm) indicated in the micrographs are presented in (b), (d), and (f), respectively.

grains.[36] The observed grain sizes are similar to those estimated from XRD line-profile analyses (results not shown).

The surface morphology of the a-Ge/Al specimen after annealing at 165 °C for 10 min is shown in the SEM micrograph presented as Fig. 3(c). The corresponding XRD measurement has indicated that the Ge layer has fully crystallized [Fig. 1(d)]. The SEM micrograph shows that the surface, which is originally made of a-Ge before annealing,

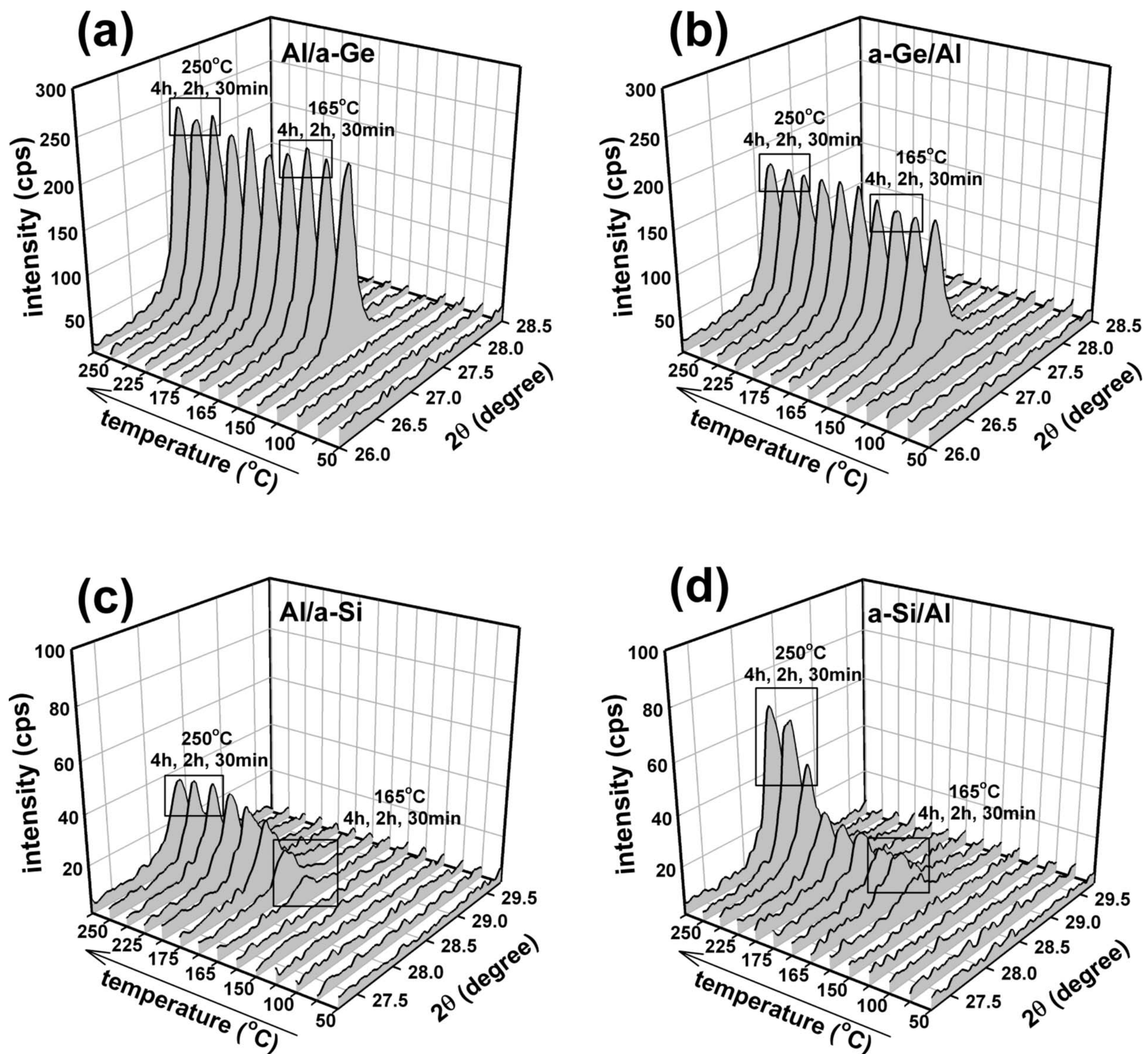

FIG. 4. [(a) and (b)] The evolution of the Ge(111) diffraction peak upon *in situ* annealing of the (a) Al/a-Ge and (b) a-Ge/Al specimens. An explosivelike, full crystallization of the a-Ge layer is observed at 150 °C for both specimens. [(c) and (d)] The evolution of the Si(111) diffraction peak upon *in situ* annealing of the (c) Al/a-Si and (d) a-Si/Al specimens. For both specimens, a gradual crystallization of a-Si is observed with increasing temperature and annealing time.

is now composed of large white areas of dendritic shape. The white dendrites are shown to be very rich in Ge by small-area AES analyses [see Fig. 3(d)]. This observation, together with the corresponding concentration-depth profile shown in Fig. 1(c), indicates that the crystallization of Ge occurs mostly in the original a-Ge layer itself. The c-Ge dendritic areas are separated by narrow dark regions, which are much richer in Al [Fig. 3(d)] than the dendritic areas.

For comparison, the surface SEM micrograph of an a-Si/Al specimen annealed at 165 °C for 3 days is shown in Fig. 3(e). The corresponding concentration-depth profile is very similar to that of the a-Ge/Al specimen annealed at 165 °C for 10 min [cf. Figs. 1(c) and 2(c)]. Evidently, the surface morphologies of the annealed a-Si/Al and a-Ge/Al specimens are very different [cf. Figs. 3(c) and 3(e)]. No dendritic areas of (c-)Si can be observed in the surface of the annealed a-Si/Al specimen. Recognizing that the corresponding XRD analysis reveals that only a *partial* crystallization of a-Si has occurred [Fig. 2(d)], it is concluded that the surface is mostly a-Si (uniform gray area) incorporating some separate Al particles [bright points, see Fig. 3(f)].

C. *In situ* x-ray diffraction results

The evolutions of the Ge(111) diffraction peaks recorded as a function of annealing temperature during *in situ* annealing of the Al/a-Ge and a-Ge/Al specimens are shown in Figs. 4(a) and 4(b), respectively. It follows that the a-Ge layers in both specimens show very similar crystallization behaviors. At temperatures below 125 °C, almost no Ge(111) diffraction peak can be detected; as the annealing temperature reaches 150 °C, a strong Ge(111) peak abruptly appears for both specimens. During the following annealing steps up to 250 °C, the Ge(111) peak intensity remains con-

stant. Hence, the entire a-Ge layer has immediately and fully crystallized at 150 °C in both specimens, irrespective of the layer sequence.

The corresponding crystallization behaviors of a-Si in the Al/a-Si and a-Si/Al specimens for the same temperatures during *in situ* annealing are shown in Figs. 4(c) and 4(d), respectively. In contrast with the "explosivelike" crystallization behavior of a-Ge in the Al/a-Ge and a-Ge/Al specimens, a gradual crystallization behavior of a-Si is observed for both Al/a-Si and a-Si/Al. Consistent with the *ex situ* observations, the crystallization kinetics of a-Si is strongly dependent on the layer sequence. For the Al/a-Si specimen [Fig. 4(c)], initial crystallization of a-Si is observed after annealing at 165 °C for as long as 2 h. With increasing temperature, the Si(111) peak shows a progressive, gradual growth. The crystallization rate is small even at a temperature as high as 250 °C. For the a-Si/Al specimen, however, initial crystallization of a-Si occurs already after 30 min of annealing at 165 °C [Fig. 4(d)]. The Si(111) peak increases with increasing annealing temperature. After 2 h at 250 °C, the Si(111) peak intensity has reached a maximum. The intensity is almost twice of that of the Al/a-Si specimen in the final stage. In this context, the results presented in Sec. III A are recalled: At 250 °C, it takes only 1 h for a-Si/Al, and a much longer time of 25 h for Al/a-Si, to achieve layer exchange of the Si and Al layers. Also, these results (see Sec. III A 2) suggest that the crystallization kinetics of a-Si correlates with the layer-exchange process of the a-Si and Al layers.

D. Summary of main experimental observations

A gradual crystallization behavior of a-Si is observed for both Al/a-Si and a-Si/Al at a temperature as low as 165 °C, and the crystallization rate of a-Si in Al/a-Si is much lower than in a-Si/Al. An explosivelike crystallization behavior of a-Ge is observed in both Al/a-Ge and a-Ge/Al layer systems at 150 °C, irrespective of the layer sequence.

The crystallization of a-Si in Al/a-Si and a-Si/Al specimens correlates with the layer-exchange process of the a-Si and Al layers.

The crystallization of a-Ge in Al/a-Ge and a-Ge/Al specimens does not correlate with such layer exchange. The a-Ge layers have fully crystallized long before layer exchange has been achieved.

The original layer sequence strongly affects the layer-exchange kinetics both in Al/Ge and in Al/Si layer systems. The layer-exchange process for Al/a-Ge is faster than that for a-Ge/Al. On the other hand, in the Al/Si layer systems, the layer-exchange process for Al/a-Si is much slower than that for a-Ge/Al.

IV. THERMODYNAMIC MODEL AND CALCULATIONS

A. Role of covalent-bond-weakening effect

The bonding in a-Si and a-Ge is strongly covalent. Therefore, homogeneous nucleation of crystallization within bulk a-Si and bulk a-Ge can only occur at relatively very high temperatures (~500 °C for a-Ge and ~700 °C for a-Si).[14] The covalent bonds in the a-Si layer or a-Ge layer are weakened at the interface with the metal layer, as a consequence of a screening effect by the free electrons in the adjacent metal layer.[28] As a result of this bond-weakening effect, the activation energy for diffusion of these interface-adjacent Si (or Ge) atoms will be lower than that of Si (or Ge) bulk atoms; i.e., these interfacial Si (or Ge) atoms gain a mobility much larger than the corresponding bulk atoms. These relatively mobile Si (or Ge) atoms can diffuse along the interface and may provide the agents for the nucleation of crystallization at much lower temperatures than holds for the corresponding bulk materials.[13,16–23] In the following, these weakly bonded interfacial Si (or Ge) atoms will be called "free" atoms. The screening effect is a very local electronic interaction, and, accordingly, the layer thickness of the free Si (or Ge) atoms is only about 1–3 ML (monolayers) adjacent to the metal layers.[28] In a soft x-ray photoemission study of Al/Si interfaces, the photoemission from the free Si interfacial layer could be distinguished from that of bulk Si.[37] Using the intensity ratio of these two types of photoelectrons, the thickness of the free silicon interfacial layer is calculated to be 4.4 Å (~2 ML Si).[38] Recognizing the (structure) similarity of Si and Ge, the thickness of the free Ge interfacial layer is also estimated to be about 2 ML at the interface with the metal.

It can be conceived that, in principle, those two metal-layer adjacent monolayers of free atoms in a-Si and a-Ge could lower the Gibbs energies of the system by, for example, (a) crystallizing, (b) dissolving into the metal layer, (c) reacting with the metal to form silicides or germanides [for example, see Ni-Si (Ref. 27)], or (d) diffusing to sites of low energy (as grain boundaries in the metal). Evidently, which process can occur depends on the competition between the change of bulk Gibbs energies and the change of corresponding surface and interface energies.

In this paper, processes as indicated above are considered for MIC processes in immiscible layer systems. For the Al/Si and Al/Ge (layer) systems, the formation of any silicide or germanide [option (c)] can be excluded based on the XRD and differential scanning calorimetry measurements performed in this work (see also Ref. 13). Furthermore, the bulk diffusion and dissolution of Si (or Ge) in Al layers are negligible at the concerned temperatures (<250 °C).[21,35] As a result, the only two options for the interfacial free Si (or Ge) atoms to lower the system Gibbs energy are (i) to crystallize at the interface with Al and/or (ii) to diffuse into Al grain boundaries ("wetting"[10]) and possibly crystallize there. For an evaluation, it then becomes indispensable to assess the values of surface and interface energies in Al/Si and Al/Ge layer systems. Therefore, in the following section, first, the corresponding surface and interface energies in Al/Si and Al/Ge layer systems will be determined employing a recently developed method.[5,31,32]

B. Evaluation of crystallization, surface, and interface energies

1. Crystallization energies

The crystallization energies ($\Delta G^{cryst}_{\langle i\rangle-\{i\}}$: the Gibbs energy difference between the crystalline and amorphous phases) of a-Ge and a-Si follow from[39]

$$\Delta G^{cryst}_{\langle i\rangle-\{i\}}(T) = \Delta H^{cryst}_{\langle i\rangle-\{i\}}(T) - T\Delta S^{cryst}_{\langle i\rangle-\{i\}}(T), \quad (1a)$$

$$\Delta H^{cryst}_{\langle i\rangle-\{i\}}(T) = \Delta H^{cryst}_{\langle i\rangle-\{i\}}(T_c) + \int_{T_c}^{T} \Delta c_p(T) dT, \quad (1b)$$

$$\Delta S^{cryst}_{\langle i\rangle-\{i\}}(T) = -S^0_{\{i\}} + \int_0^T \frac{\Delta c_p(T)}{T} dT. \quad (1c)$$

Here, i represents Ge or Si, $\langle\,\rangle$ stands for the crystalline phase, and $\{\,\}$ represents the amorphous phase. T_c stands for the crystallization temperature at which the crystallization enthalpy $\Delta H^{cryst}_{\langle i\rangle-\{i\}}$ was measured. $\Delta c_p(T)$ is the specific heat difference between the crystalline and amorphous phases, and $S^0_{\{i\}}$ is the residual entropy of the amorphous phase at 0 K. Using the thermodynamic values summarized in Ref. 39, the crystallization energies of both a-Ge and a-Si have been calculated as a function of temperature. The results are shown in Fig. 5(a). It follows that the crystallization energy of a-Si is more negative (i.e., more energy is released upon crystallization) than that of a-Ge. Both crystallization energies decrease with increasing temperature.

2. Surface energies

The Gibbs surface energy $G^S_{\langle A\rangle}$ (in J/mol) of a crystalline surface $\langle A\rangle$ at temperature T can be expressed in terms of the surface enthalpy $H^S_{\langle A\rangle}$ and the surface entropy $S^S_{\langle A\rangle}$:

$$G^S_{\langle A\rangle}(T) = H^S_{\langle A\rangle} - TS^S_{\langle A\rangle}. \quad (2)$$

Similarly, the Gibbs surface energy $G^S_{\{A\}}$ of an amorphous[40] surface $\{A\}$ is given by

$$G^S_{\{A\}}(T) = H^S_{\{A\}} - TS^S_{\{A\}}. \quad (3)$$

The surface entropies $S^S_{\langle A\rangle}$ and $S^S_{\{A\}}$ are approximately equal to 7.72 and 7.34 J mol^{-1} K^{-1}, respectively, based on relevant experimental data.[30,31]

The corresponding Gibbs surface energies per unit area $\gamma^S_{\langle A\rangle}$ and $\gamma^S_{\{A\}}$ (in J/m^2) are given by[30]

$$\gamma^S_{\langle A\rangle}(T) = \frac{H^S_{\langle A\rangle} - TS^S_{\langle A\rangle}}{f_{\langle A\rangle} C_0 V^{2/3}_{\langle A\rangle}}, \quad (2')$$

$$\gamma^S_{\{A\}}(T) = \frac{H^S_{\{A\}} - TS^S_{\{A\}}}{f_{\{A\}} C_0 V^{2/3}_{\{A\}}}, \quad (3')$$

where $V_{\langle A\rangle}$ and $V_{\{A\}}$ stand for the molar volumes of $\langle A\rangle$ and $\{A\}$; $f_{\langle A\rangle}$ and $f_{\{A\}}$ represent the average fraction of the surface of an atomic cell in contact with vacuum ($f_{\langle A\rangle}$=0.35, $f_{\{A\}}$=0.33);[30] C_0 is a constant relating the surface area to the corresponding bulk volume, with an average value of 4.5×10^8 mol$^{-1/3}$.[30]

With known experimental values of $\gamma^S_{\langle A\rangle}(T_0)$ and $\gamma^S_{\{A\}}(T_0)$ at a temperature T_0, the surface energies of $\langle A\rangle$ and $\{A\}$ at a temperature T can be calculated on the basis of Eqs. (2′) and (3′), respectively,

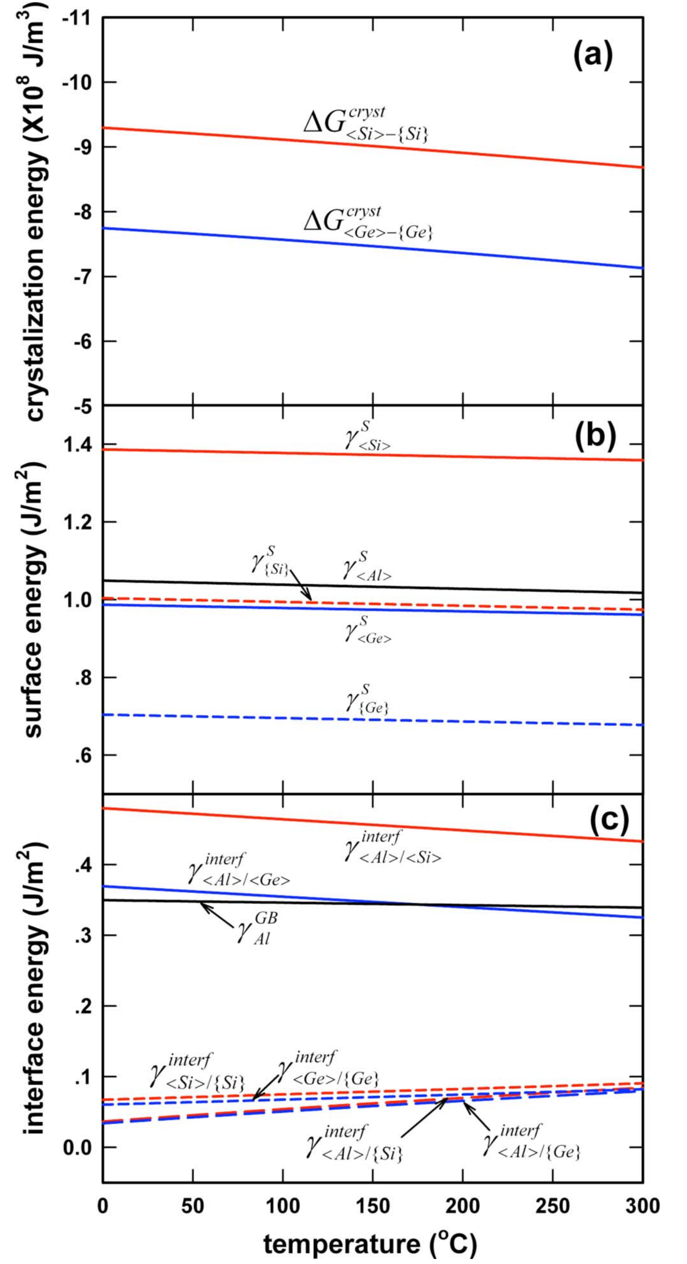

FIG. 5. (Color online) Calculated (a) crystallization energies, (b) surface energies, and (c) interface energies related to the Al/Si and Al/Ge layer systems. The calculation methods have been discussed in detail in the text.

$$\gamma^S_{\langle A\rangle}(T) = \frac{(\gamma^S_{\langle A\rangle}(T_0) f_{\langle A\rangle} C_0 V^{2/3}_{\langle A\rangle} + T_0 S^S_{\langle A\rangle}) - TS^S_{\langle A\rangle}}{f_{\langle A\rangle} C_0 V^{2/3}_{\langle A\rangle}}, \quad (2'')$$

$$\gamma^S_{\{A\}}(T) = \frac{(\gamma^S_{\{A\}}(T_0) f_{\{A\}} C_0 V^{2/3}_{\{A\}} + T_0 S^S_{\{A\}}) - TS^S_{\{A\}}}{f_{\{A\}} C_0 V^{2/3}_{\{A\}}}. \quad (3'')$$

Using Eqs. (2″) and (3″), the surface energies of c-Si, a-Si, c-Ge, a-Ge, and c-Al at temperatures between 0 and 300 °C have been calculated; results are shown in Fig. 5(b). The parameters that were employed for the calculations have been summarized in Table I.[41–46] It can be noticed that the

TABLE I. Parameters for surface energy calculations [$\langle\,\rangle$, crystalline surface; $\{\,\}$, amorphous (liquid) surface; $\gamma^S(T_0)$, experimental surface energy at measurement temperature T_0; V_m, molar volume (from Ref. 41)].

	⟨Si⟩	{Si}	⟨Ge⟩	{Ge}	⟨Al⟩
$\gamma^S(T_0)$ (J m^{-2})	1.37[a]	0.87[b]	0.97[a]	0.62[b]	1.03[c]
T_0 (K)	493	1685	473	1211	500
V_m ($\times 10^{-6}$ m^3 mol^{-1})	12.13	11.10	13.65	12.97	10.06

[a]From Ref. 42; see also Refs. 30 and 44.
[b]From Ref. 43; see also Refs. 41 and 45.
[c]From Ref. 42; see also Refs. 30 and 46.

surface energy of the amorphous phases ({Si}, {Ge}) is significantly lower than that of the corresponding crystalline phases (⟨Si⟩, ⟨Ge⟩).

3. Interface energies

As compared with surface energies, it is much more difficult to directly measure energies of interfaces between various crystalline and amorphous phases. However, theoretical evaluations of interface energies based on universal thermodynamic models and available thermodynamic data have been successfully developed in recent years.[1,30] Recently, departing from Refs. 5 and 30, the interface thermodynamic model was extended and improved.[31] In the present work, the corresponding interfacial energies have therefore been calculated with the improved thermodynamic model.

For the *interface between two crystalline phases* $\langle A\rangle$ and $\langle B\rangle$, the interfacial Gibbs energy $G^{interf}_{\langle A\rangle/\langle B\rangle}$ (in J/mol) is given by[30]

$$G^{interf}_{\langle A\rangle/\langle B\rangle} = G^{mis}_{\langle A\rangle/\langle B\rangle} + G^{chem}_{\langle A\rangle/\langle B\rangle}. \tag{4a}$$

The interfacial mismatch energy $G^{mis}_{\langle A\rangle/\langle B\rangle}$ is due to the mismatch between the lattices of $\langle A\rangle$ and $\langle B\rangle$ at the interface and may comprise energy contributions due to elastic strain and possible dislocations.[33] $G^{mis}_{\langle A\rangle/\langle B\rangle}$ can be estimated by[5,31]

$$G^{mis}_{\langle A\rangle/\langle B\rangle} = \frac{1}{3}\left(\frac{G^S_{\langle A\rangle} + G^S_{\langle B\rangle}}{2}\right), \tag{4b}$$

where $G^S_{\langle A\rangle}$ and $G^S_{\langle B\rangle}$ are the Gibbs surface energies of $\langle A\rangle$ and $\langle B\rangle$, respectively. As a particular case, the energy of a high-angle grain boundary in $\langle A\rangle$, i.e., an $\langle A\rangle/\langle A\rangle$ homophase interface, $G^{GB}_{\langle A\rangle}$ is assessed by

$$G^{GB}_{\langle A\rangle} = \frac{1}{3}G^S_{\langle A\rangle}. \tag{4c}$$

The interfacial chemical energy $G^{chem}_{\langle A\rangle/\langle B\rangle}$, which represents the chemical interaction between $\langle A\rangle$ and $\langle B\rangle$, is given by

$$G^{chem}_{\langle A\rangle/\langle B\rangle} = H^{chem}_{\langle A\rangle/\langle B\rangle} - TS^{chem}_{\langle A\rangle/\langle B\rangle}, \tag{4d}$$

where the enthalpy contribution $H^{chem}_{\langle A\rangle/\langle B\rangle}$ is related to the partial enthalpy of $\langle A\rangle$ in $\langle B\rangle$ at infinite dilution $\Delta H^0_{\langle A\rangle \text{ in } \langle B\rangle}$ and of $\langle B\rangle$ in $\langle A\rangle$ at infinite dilution $\Delta H^0_{\langle B\rangle \text{ in } \langle A\rangle}$,[31]

$$H^{chem}_{\langle A\rangle/\langle B\rangle} = f_{\langle j\rangle}\left(\frac{\Delta H^0_{\langle A\rangle \text{ in } \langle B\rangle} + \Delta H^0_{\langle B\rangle \text{ in } \langle A\rangle}}{2}\right). \tag{4e}$$

Here, $f_{\langle j\rangle}=f_{\langle A\rangle}=f_{\langle B\rangle}=0.35$ [see below Eq. (3″)].

The interfacial chemical entropy $S^{chem}_{\langle A\rangle/\langle B\rangle}$ is assessed by[31]

$$S^{chem}_{\langle A\rangle/\langle B\rangle} = f_{\langle j\rangle}\left(3R\ln\frac{\prod_j \Theta_j^{1/2}}{\sum_j \frac{1}{2}\Theta_j + \Delta\Theta_{interf}}\right), \tag{4f}$$

where Θ_j stands for the Debye temperature of component j ($\langle A\rangle$ or $\langle B\rangle$). $\Delta\Theta_{interf}$ is the Debye temperature change of the interface atoms (taking atom-type independent) with respect to the Debye temperature of the bulk atoms, and is estimated by

$$\Delta\Theta_{interf} = 34.1\times 10^{-3}\left(-\frac{\Delta H_{\langle AB\rangle}}{R}\right), \tag{4g}$$

with $\Delta H_{\langle AB\rangle}$ as the enthalpy of formation of the $\langle AB\rangle$ solid solution and R as the gas constant.

Finally, the interfacial Gibbs energy per unit area (in J/m^2) can be calculated from

$$\gamma^{interf}_{\langle A\rangle/\langle B\rangle} = \frac{G^{interf}_{\langle A\rangle/\langle B\rangle}}{f_{\langle A\rangle}C_0\bar{V}^{2/3}_{\langle A\rangle-\langle B\rangle}}, \tag{4h}$$

where $\bar{V}_{\langle A\rangle-\langle B\rangle}$ stands for the average molar volume of $\langle A\rangle$ and $\langle B\rangle$.

For the *interface between a crystalline phase* $\langle A\rangle$ *and an amorphous phase* $\{B\}$,[40] the interfacial Gibbs energy $G^{interf}_{\langle A\rangle/\{B\}}$ is

$$G^{interf}_{\langle A\rangle/\{B\}} = H^{interf}_{\langle A\rangle/\{B\}} - TS^{interf}_{\langle A\rangle/\{B\}} \tag{5a}$$

with a total interface enthalpy contribution $H^{interf}_{\langle A\rangle/\{B\}}$ according to[31]

$$H^{interf}_{\langle A\rangle/\{B\}}(T) = f_{\{A\}}\times\left[H_{\{A\}}(T) - H_{\langle A\rangle}(T) + \frac{\Delta H^0_{\{A\} \text{ in } \{B\}} + H_{\{B\}}(T) - H_{\langle B\rangle}(T) + \Delta H^0_{\{B\} \text{ in } \{A\}} + H_{\{A\}}(T) - H_{\langle A\rangle}(T)}{2}\right]. \tag{5b}$$

TABLE II. Parameters for interface energy calculations (Refs. 41, 47, and 48).

$\Delta H^0_{\langle Al\rangle \text{ in } \langle Ge\rangle}$	$\Delta H^0_{\langle Ge\rangle \text{ in } \langle Al\rangle}$	$\Delta H^0_{Ge(diam)\to Ge(fcc)}$	$\Delta S_{Ge(diam)\to Ge(fcc)}$	$\Delta H^0_{\{Al\} \text{ in } \{Ge\}}$ $\Delta H^0_{\{Ge\} \text{ in } \{Al\}}$	Θ_{Ge}	Θ_{Al}
32857 J mol^{-1}	−3143 J mol^{-1}	36000 J mol^{-1}	22.3 J mol^{-1} K^{-1}	−11304 J mol^{-1}	374 K	428 K
$\Delta H^0_{\langle Al\rangle \text{ in } \langle Si\rangle}$	$\Delta H^0_{\langle Si\rangle \text{ in } \langle Al\rangle}$	$\Delta H^0_{Si(diam)\to Si(fcc)}$	$\Delta S_{Si(diam)\to Si(fcc)}$	$\Delta H^0_{\{Al\} \text{ in } \{Si\}}$ $\Delta H^0_{\{Si\} \text{ in } \{Al\}}$	Θ_{Si}	$\Delta H^m_{\{Al\}}$
47857 J mol^{-1}	−3143 J mol^{-1}	51000 J mol^{-1}	21.8 J mol^{-1} K^{-1}	−11340 J mol^{-1}	645 K	10784.4 J mol^{-1}

The interface entropy $S^{interf}_{\langle A\rangle/\{B\}}$ is given by[5]

$$S^{interf}_{\langle A\rangle/\{B\}} = -0.678R. \tag{5c}$$

The interface energy per unit area can finally be calculated from

$$\gamma^{interf}_{\langle A\rangle/\{B\}} = \frac{G^{interf}_{\langle A\rangle/\{B\}}}{f_{\{A\}} C_0 \bar{V}^{2/3}_{\langle A\rangle-\{B\}}}, \tag{5d}$$

where $\bar{V}_{\langle A\rangle-\{B\}}$ stands for the average molar volume of $\langle A\rangle$ and $\{B\}$.

The thus calculated interface energies of $\langle Al\rangle/\langle Ge\rangle$, $\langle Al\rangle/\{Ge\}$, $\langle Ge\rangle/\{Ge\}$, $\langle Al\rangle/\langle Si\rangle$, $\langle Al\rangle/\{Si\}$, and $\langle Si\rangle/\{Si\}$ and the grain boundary energy of Al are shown as a function of temperature in Fig. 5(c). The thermodynamic parameters used for the calculations have been gathered in Table II.[41,47,48] From the calculated interface energies, an important observation can be made: The energy of crystalline/amorphous interfaces (for example, $\langle Al\rangle/\{Ge\}$ and $\langle Al\rangle/\{Si\}$) is much lower than that of the corresponding crystalline/crystalline interfaces ($\langle Al\rangle/\langle Ge\rangle$ and $\langle Al\rangle/\langle Si\rangle$).

C. Thermodynamics of metal-induced crystallization processes

1. Grain boundary wetting

Grain boundary wetting by a phase is possible as long as the total interface energy can be reduced by replacing the GB with two interphase boundaries.[9–11] Within this context, the possibility of diffusion of free Ge or Si atoms into Al grain boundaries can be investigated. A comparison between the interface energies of Al GB (γ^{GB}_{Al}) and two times the $\langle Al\rangle/\{Ge\}$ or $\langle Al\rangle/\{Si\}$ interphase boundaries ($2\gamma^{interf}_{\langle Al\rangle/\{Ge\}}$ or $2\gamma^{interf}_{\langle Al\rangle/\{Si\}}$) is provided in Fig. 6(a). It follows that the diffusion of Ge or Si atoms into Al GBs (i.e., wetting) is favored because this reduces the Gibbs energy of the system. The driving forces $\Delta\gamma_D^{\text{Ge in Al GB}}$ and $\Delta\gamma_D^{\text{Si in Al GB}}$ for the diffusion of Ge and Si atoms into Al GBs are given by[10,11]

$$\Delta\gamma_D^{\text{Ge in AlGB}} = \gamma^{GB}_{Al} - 2\gamma^{interf}_{\langle Al\rangle/\{Ge\}},$$

$$\Delta\gamma_D^{\text{Si in AlGB}} = \gamma^{GB}_{Al} - 2\gamma^{interf}_{\langle Al\rangle/\{Si\}}. \tag{6}$$

A positive driving force equal to about 0.22 J/m^2 (at 150 °C) exists for both a-Ge and a-Si [Fig. 6(a)], with the driving force for a-Ge being slightly larger than that for a-Si. The a-Ge or a-Si wetting layer realizes a "splitting" of the Al GBs and allows Ge or Si atoms to diffuse along the Al GBs through the whole Al layer [see Fig. 3(a) and its discussion; for atomic scale evidence by TEM, see Ref. 13].

2. Interface and grain boundary nucleation of crystallization

As discussed at the start of Sec. IV A, homogeneous nucleation of crystallization within a-Ge or a-Si is impossible at low temperatures. Yet, low-temperature nucleation of c-Ge or c-Si could occur heterogeneously at the interface with Al and/or at the Al GBs, where free Ge or Si atoms are present due to the covalent-bond-weakening effect (see Sec. IV A) and the GB wetting (see Sec. IV C 1). A factor obstructing the nucleation of crystallization at interfaces is that the energy of crystalline/amorphous interfaces is usually lower than that of corresponding crystalline/crystalline interfaces [see Fig. 5(c)]. Consequently, a thin amorphous layer is often thermodynamically stable at surfaces and interfaces until reaching a critical thickness (this has first been recognized in Ref. 5; see also Refs. 32 and 33). Considering the wetting a-Ge or a-Si layer at the Al GBs, the critical thickness for the nucleation of crystallization can now be calculated by dividing the increase of interface energy due to crystallization (in J/m^2) by the bulk crystallization energy (in J/m^3),

$$h^{crit}_{\text{Ge in AlGB}} = \frac{2\times(\gamma^{interf}_{\langle Al\rangle/\langle Ge\rangle} - \gamma^{interf}_{\langle Al\rangle/\{Ge\}})}{-\Delta G^{cryst}_{\langle Ge\rangle-\{Ge\}}},$$

$$h^{crit}_{\text{Si in AlGB}} = \frac{2(\gamma^{interf}_{\langle Al\rangle/\langle Si\rangle} - \gamma^{interf}_{\langle Al\rangle/\{Si\}})}{-\Delta G^{cryst}_{\langle Si\rangle-\{Si\}}}. \tag{7}$$

The free Ge or Si atoms could also crystallize directly at the original $\langle Al\rangle/\{Ge\}$ or $\langle Al\rangle/\{Si\}$ interfaces. The critical thickness for this crystallization process is given by

$$h^{crit}_{\langle Al\rangle/\{Ge\}} = \frac{\gamma^{interf}_{\langle Al\rangle/\langle Ge\rangle} + \gamma^{interf}_{\langle Ge\rangle/\{Ge\}} - \gamma^{interf}_{\langle Al\rangle/\{Ge\}}}{-\Delta G^{cryst}_{\langle Ge\rangle-\{Ge\}}},$$

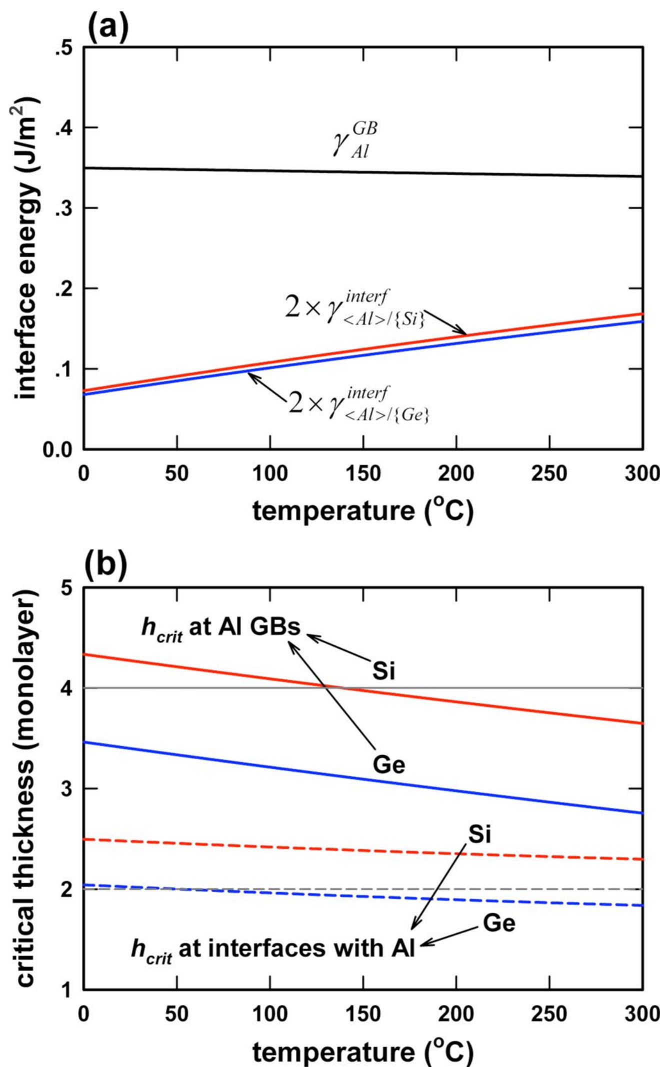

FIG. 6. (Color online) (a) Energetics of the Al grain boundary wetting by a-Ge and a-Si. A positive driving force $\gamma_{\mathrm{Al}}^{GB} - 2\gamma_{\langle\mathrm{Al}\rangle/\{\mathrm{Ge\ or\ Si}\}}^{interf}$ is evident for both Ge and Si to diffuse into the Al grain boundaries (wetting). (b) Energetics of the nucleation of crystalline Ge (and Si) at the Al GBs and at the Al/a-Ge and Al/a-Si interfaces. Note that the thicknesses of the free Ge or Si layers are about 2 ML at the interfaces with Al and ~4 ML at the Al GBs (both these thicknesses are shown by gray, horizontal lines in the figure). It follows that c-Ge can nucleate both at the Al GBs and Al/a-Ge interfaces (above 50 °C), whereas c-Si can nucleate only at the Al GBs (above 140 °C).

$$h_{\langle\mathrm{Al}\rangle/\{\mathrm{Si}\}}^{crit} = \frac{\gamma_{\langle\mathrm{Al}\rangle/\langle\mathrm{Si}\rangle}^{interf} + \gamma_{\langle\mathrm{Si}\rangle/\{\mathrm{Si}\}}^{interf} - \gamma_{\langle\mathrm{Al}\rangle/\{\mathrm{Si}\}}^{interf}}{-\Delta G_{\langle\mathrm{Si}\rangle-\{\mathrm{Si}\}}^{cryst}}. \quad (8)$$

On the basis of the calculated crystallization energies and interface energies (Fig. 5), the critical thicknesses for the initiation of crystallization of a-Ge and a-Si at the Al GBs and at the interfaces with Al were calculated applying Eqs. (7) and (8). The results are shown in Fig. 6(b) (the unit is ML where 1 ML Si ~ 2.2 Å and 1 ML Ge ~ 2.5 Å).[38] For a-Ge, the critical thickness is below 2 ML at the Al/a-Ge interface (above 50 °C). As discussed above, the thickness of the free Ge layer at the interface with Al is 2 ML, which is above the critical thickness for crystallization. Therefore, the free Ge layers can crystallize at the Al/a-Ge interfaces at low temperatures, in accordance with TEM observations reported in Refs. 15 and 22. At the Al GBs, the Ge layer is sandwiched between two Al grains and, consequently, the total thickness of free Ge at the Al GBs is 4 ML. According to Fig. 6(b), the critical thickness for the crystallization of a-Ge at the Al GBs varies from about 3.5 ML at 0 °C to about 2.8 ML at 300 °C. Hence, the initiation of the crystallization of a-Ge can also occur at the Al GBs.

For a-Si, the critical thickness for crystallization at the Al/a-Si interface is above 2 ML even at 300 °C. Therefore, the 2 ML of free Si at the interface would prefer to stay amorphous and the initiation of crystallization cannot occur at this location. At the Al GBs, the critical thickness for the initiation of crystallization is below 4 ML at temperatures above 140 °C. Hence, the only site for c-Si to nucleate at low temperatures is the Al grain boundary, and the crystallization temperature should be higher than 140 °C for the Al/a-Si layer system (the experimental work performed in this project indicates a minimal crystallization temperature of about 165 °C; see Sec. III C). TEM evidence for the crystallization of a-Si at Al GBs (at 175 °C) is given in Ref. 13. Furthermore, a recent experimental study has confirmed that Al-induced crystallization of a-Si is initiated *exclusively* at the Al GBs (and not at the original Al/a-Si interface).[21]

3. Continued crystallization

It has been shown above for the Al/a-Si system that the only site for the nucleation of crystallization is at the Al GBs. After the initiation of the crystallization of a-Si, every wetted Al GB in the Al layer is replaced by two ⟨Al⟩/⟨Si⟩ interphase boundaries. To proceed with the crystallization process of a-Si, the Si atoms in the a-Si layer must continue to diffuse now into the ⟨Al⟩/⟨Si⟩ interphase boundaries (wetting) and crystallize there. The driving force for the diffusion $\Delta\gamma_D^{\mathrm{Si\ in}\ \langle\mathrm{Al}\rangle/\langle\mathrm{Si}\rangle}$ is given by

$$\Delta\gamma_D^{\mathrm{Si\ in}\ \langle\mathrm{Al}\rangle/\langle\mathrm{Si}\rangle} = \gamma_{\langle\mathrm{Al}\rangle/\langle\mathrm{Si}\rangle}^{interf} - (\gamma_{\langle\mathrm{Al}\rangle/\{\mathrm{Si}\}}^{interf} + \gamma_{\langle\mathrm{Si}\rangle/\{\mathrm{Si}\}}^{interf}). \quad (9a)$$

As follows from Fig. 7(a), this driving force is (also) positive (~0.3 J/m^2 at 150 °C), indicating that a-Si is capable (to continue) of wetting the ⟨Al⟩/⟨Si⟩ boundaries.

Considering the wetting a-Si layer at the ⟨Al⟩/⟨Si⟩ interphase boundaries, two cases are possible: (i) The wetting a-Si layer joins with the adjacent c-Si grains to crystallize, as a result of which the c-Si grains grow *laterally*, perpendicular to the ⟨Al⟩/⟨Si⟩ boundaries. (ii) New grains of c-Si nucleate. The critical thickness in case (i), i.e., for continued lateral c-Si grain growth perpendicular to the ⟨Al⟩/⟨Si⟩ boundaries, is given by

$$h_{\mathrm{Si\ grain\ growth}}^{crit} = \frac{\gamma_{\langle\mathrm{Al}\rangle/\langle\mathrm{Si}\rangle}^{interf} - (\gamma_{\langle\mathrm{Al}\rangle/\{\mathrm{Si}\}}^{interf} + \gamma_{\langle\mathrm{Si}\rangle/\{\mathrm{Si}\}}^{interf})}{-\Delta G_{\langle\mathrm{Si}\rangle-\{\mathrm{Si}\}}^{cryst}}. \quad (9b)$$

The critical thickness in case (ii), i.e., for the formation of new c-Si grains at the ⟨Al⟩/⟨Si⟩ boundaries, is given by

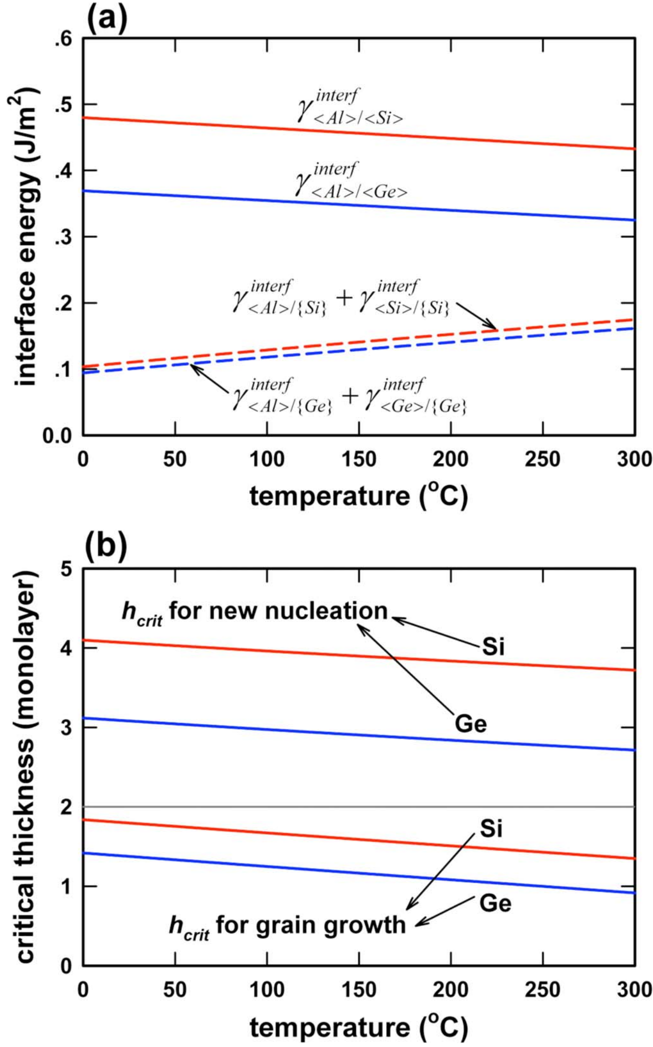

FIG. 7. (Color online) (a) Energetics of the continued diffusion of Ge and Si atoms into the Al layer after completing the initial nucleation of the crystallization process at the Al GBs. A positive driving force is present for both Ge and Si for continued diffusion into the ⟨Al⟩/⟨Ge⟩ and ⟨Al⟩/⟨Si⟩ boundaries, respectively. (b) Energetics for continued lateral grain growth of c-Ge and c-Si in the original Al layer (perpendicular to the original Al GBs). Continued grain growth, rather than repeated nucleation of crystallization, is favored for both Ge and Si. The formation of new crystalline nuclei is impossible.

$$h^{crit}_{\text{Si new nucleation}} = \frac{\gamma^{interf}_{\langle \text{Al}\rangle/\langle \text{Si}\rangle} + \gamma^{interf}_{\langle \text{Si}\rangle/\langle \text{Si}\rangle} - (\gamma^{interf}_{\langle \text{Al}\rangle/\{\text{Si}\}} + \gamma^{interf}_{\langle \text{Si}\rangle/\{\text{Si}\}})}{-\Delta G^{cryst}_{\langle \text{Si}\rangle - \{\text{Si}\}}}. \tag{9c}$$

The calculation results are shown in Fig. 7(b). The critical thickness for the formation of new c-Si nuclei [Eq. (9c)] is as large as ∼4 ML. Recognizing that the thickness of the free Si atoms adjacent to Al is only about 2 ML, it follows that the formation of new c-Si nuclei at the ⟨Al⟩/⟨Si⟩ boundaries is impossible. The critical thickness for continued c-Si grain growth [Eq. (9b)] is only ∼1.5 ML (at $T>150$ °C). Hence, continued lateral growth of the c-Si grains initially formed at the original Al GBs is possible, which is in accordance with the *in situ* and *ex situ* TEM analyses (i.e., only c-Si grain growth at initially formed ⟨Al⟩/⟨Si⟩ interfaces is observed).[13] Additionally, recognizing the large positive driving force $\Delta\gamma_D^{\text{Si in }\langle\text{Al}\rangle/\langle\text{Si}\rangle}$ for Si atoms diffusing into the ⟨Al⟩/⟨Si⟩ boundaries, this result strongly indicates that the lateral growth of the initially nucleated c-Si grains at the original Al GBs is realized by continuously incorporating Si atoms diffusing from the a-Si layer into the ⟨Al⟩/⟨Si⟩ boundaries.

The continuous inward diffusion and crystallization (grain growth) of Si within the original Al GBs can result in (i) free space left in the original a-Si layer; (ii) compressive stress built up in the Al grains. As a result of both effects, it is suggested that Al tends to occupy the free space in the Si layer to relax the stress (the *in situ* x-ray diffraction stress measurements performed in this project indicated that, indeed, the Al phase maintains a low level of compressive stress during MIC). Thus, the Al layer is gradually "displaced" by the growing c-Si grains and "moves" to the original location of the a-Si layer. As a consequence of this process, a continuous c-Si layer is formed at the position of the original Al layer: layer exchange. Thereby, the correlation of layer exchange and crystallization of the a-Si phase has been explained. Moreover, due to the thermodynamic impossibility of new c-Si nucleation after the initial nucleation of c-Si at Al GBs, it follows that the final lateral c-Si grain sizes are similar to the original Al lateral grain sizes, which is in agreement with observations in Al/Si layer systems.[16–18]

In contrast with the Al/a-Si layer system, crystalline Ge can nucleate both at the Al GBs and at the interface with the Al layer (Sec. IV C 2). The two possible cases of continued crystallization of a-Ge at the original Al GBs can be considered similarly as for the Al/a-Si system; thus [see Eqs. (9a)–(9c)],

$$\Delta\gamma_D^{\text{Ge in }\langle\text{Al}\rangle/\langle\text{Ge}\rangle} = \gamma^{interf}_{\langle \text{Al}\rangle/\langle \text{Ge}\rangle} - (\gamma^{interf}_{\langle \text{Al}\rangle/\{\text{Ge}\}} + \gamma^{interf}_{\langle \text{Ge}\rangle/\{\text{Ge}\}}), \tag{10a}$$

$$h^{crit}_{\text{Ge grain growth}} = \frac{\gamma^{interf}_{\langle \text{Al}\rangle/\langle \text{Ge}\rangle} - (\gamma^{interf}_{\langle \text{Al}\rangle/\{\text{Ge}\}} + \gamma^{interf}_{\langle \text{Ge}\rangle/\{\text{Ge}\}})}{-\Delta G^{cryst}_{\langle \text{Ge}\rangle - \{\text{Ge}\}}}, \tag{10b}$$

$$h^{crit}_{\text{Ge new nucleation}} = \frac{\gamma^{interf}_{\langle \text{Al}\rangle/\langle \text{Ge}\rangle} + \gamma^{interf}_{\langle \text{Ge}\rangle/\langle \text{Ge}\rangle} - (\gamma^{interf}_{\langle \text{Al}\rangle/\{\text{Ge}\}} + \gamma^{interf}_{\langle \text{Ge}\rangle/\{\text{Ge}\}})}{-\Delta G^{cryst}_{\langle \text{Ge}\rangle - \{\text{Ge}\}}}. \tag{10c}$$

The calculation results are also shown in Figs. 7(a) and 7(b). It follows that a-Ge is capable of wetting the ⟨Al⟩/⟨Ge⟩ boundaries ($\Delta\gamma_D^{\text{Ge in }\langle\text{Al}\rangle/\langle\text{Ge}\rangle}>0$) and subsequently crystallizes there by joining the preexisting c-Ge nuclei ($h^{crit}_{\text{Ge grain growth}}\sim 1$ ML), thereby establishing lateral growth of the initially nucleated c-Ge grains. Similar to the Al/a-Si layer system, the formation of new c-Ge nuclei at the ⟨Al⟩/⟨Ge⟩ boundaries is impossible ($h^{crit}_{\text{Ge new nucleation}}\sim 3$ ML). Since c-Ge is also capable of nucleating at the Al/a-Ge interface, c-Ge grain growth can also occur at the same time within the a-Ge layer itself starting from the c-Ge grains

nucleated at the interface. The interface-mediated and GB-mediated crystallizations of a-Ge occur simultaneously. As a result, the a-Ge phase is very fastly fully crystallized, long before a complete layer exchange as induced by crystallization at the original Al GBs has been realized. The morphology of c-Ge crystallized within the original Al sublayer is shown in Fig. 3(a). The branchlike c-Ge grains were formed between Al grains (see Sec. III B). The dendritic crystallization morphology of c-Ge initiated at the Al/Ge interface is shown in Fig. 3(c) for a fully crystallized specimen (see also the corresponding TEM observations in Refs. 15 and 22). It can also be noticed that a small amount of Al diffuses along the boundaries of the Ge crystallites to the surface during MIC. Because interface-mediated crystallization of a-Si is absent for the Al/Si system, the resulting morphology is very different from that observed for the Al/Ge system; see Fig. 3(e) for an annealed *a*-Si/Al specimen, which has partially crystallized after 3 days at 165 °C (see Fig. 2).

D. Discussion and remarks on layer exchange

According to the thermodynamic model calculations, the most striking difference between the Al/Ge and Al/Si layer systems is that c-Ge can (also) nucleate at the Al/a-Ge interface, whereas c-Si cannot nucleate at the Al/a-Si interface. Al GBs are preferred sites for crystallite nucleation and subsequent lateral growth in both layer systems. These predictions are in very good agreement with the experimental observations obtained in this work and discussed in Sec. III, and also with results from other research groups: Almost all results on MIC in the Al/Si layer system indicate that MIC in Al/Si is associated with a layer exchange of Al and Si.[16–19] Initial nucleation of c-Si was found to occur within the Al layer.[13,14,17] In the few studies on MIC in the Al/Ge layer system, MIC behaviors different from that of Al/Si were reported.[15,22] The nucleation of c-Ge at the Al/a-Ge interface was observed.[15,22] Hence, the predictions of the thermodynamic model are validated by the corresponding experimental data on the Al/Ge and Al/Si systems.

Whereas full crystallization of a-Si in Al/a-Si (a-Si/Al) occurs in association with layer exchange, full crystallization of a-Ge in Al/a-Ge (a-Ge/Al) is realized without achieving such layer exchange. Then, it is important to note that a layer exchange of Al and Ge layers, similar to that observed for the Al/Si system, *does* occur upon further annealing, after full crystallization of the a-Ge layer (see. Fig. 1). Hence, in this case, layer exchange involves *crystalline* Al and *crystalline* Ge layers. Further, the kinetics of the layer-exchange process in the Al/Ge layer system is dependent on the original layer sequence; such dependence was also observed for the Al/Si layer system (see. Figs. 1 and 2).

Layer exchange of crystalline Au and crystalline Si layers has previously been observed upon annealing a c-Au/c-Si bilayer specimen at temperatures below 300 °C.[49] The process would involve the development of large c-Si grains within the c-Au layer; the resulting decrease in c-Si GB density and thus energy would drive the layer exchange. It may then be suggested that, similarly, the layer exchange of c-Al and c-Ge layers results from the development of large c-Ge grains within the c-Al layer. Because the surface energy of c-Ge is lower than that of c-Al [see Fig. 5(b)], it may be expected that the development of c-Ge grains within the c-Al layer (and the replacement of Al) is more favorable if the original Al layer is on the top of the specimen,[50] which is consistent with the observed difference in layer-exchange kinetics of Al/a-Ge and a-Ge/Al. Besides, the layer-exchange process could also be promoted by the stress relaxation in the c-Al and c-Ge phases upon layer exchange.[18]

In the case of the Al/Si layer system, the layer-exchange process for Al/a-Si is much slower than that for a-Si/Al. In this case, the stress relaxation in and the grain growth of the Al phase control the kinetics of layer exchange.[18,20] The driving force for layer exchange was calculated to be larger for a-Si/Al than for Al/a-Si, in agreement with the observed difference in the layer-exchange kinetics.[20]

E. Model calculations for the Au/a-Si and Ag/a-Si systems

The model is, in principle, applicable to MIC processes in all immiscible alloy systems. Thus, results of the application of the model to the Ag/a-Si and Au/a-Si systems are shown in Fig. 8. The thermodynamic parameters needed for the calculations can be found in Refs. 47, 51, and 52. Similar to the Al/a-Si system, a-Si is capable of wetting also the Au GBs and Ag GBs [Fig. 8(a)]. Note that there is, in particular, a very large driving force for a-Si to wet the Au GBs ($\sim$0.5 J/m^2); the driving force for a-Si to wet the Ag GBs is much smaller ($\sim$0.1 J/m^2).

Now, consider the nucleation of crystallization of a-Si in Ag/a-Si and Au/a-Si systems. Following from Fig. 8(b), the critical thickness for a-Si to crystallize at Ag GBs is lower than 4 ML for a temperature larger than about 400 °C, whereas at the Ag/a-Si interface, the critical thickness for the crystallization of a-Si is about 2.5 ML (>2 ML). Hence, with reference to the discussion in Sec. IV C 2, it can be predicted that the MIC in the Ag/a-Si system will occur at a minimal temperature close to 400 °C; in particular, the crystallization will be initiated at Ag GBs. This predicted MIC behavior agrees very well with the experimental result in the Ag/a-Si layer system: The crystallization of a-Si starts within the Ag layer at 390–410 °C.[14]

For the Au/a-Si system, the model calculation shows that the critical thickness for the nucleation of crystallization of a-Si is $\sim$5.5 to 6 ML at Au GBs (for $T<400$ °C) and $\sim$3.3 ML at the Au/a-Si interface. Hence, the direct (i.e., without the aid of an intermediate phase; see below) crystallization of a-Si in the Au/Si system is unlikely, in any case at temperature below 400 °C. However, the reported MIC temperature of the Au/a-Si system is only 100–200 °C.[14,25] It appears that MIC in the Au/a-Si system is mediated by the formation of an *intermediate* metastable phase (there is no stable intermetallic phase in the Au-Si system), as suggested by experimental observations. It was found that Si penetration into Au GBs occurred at 100 °C and that metastable crystalline Au_3Si nucleated at Au GBs at $\sim$100 °C.[25] Continued lateral growth of c-Au_3Si perpendicular to the Au GBs was also observed.[25] In order to understand the formation of Au_3Si, calculations on the possible nucleation of Au_3Si at the Au

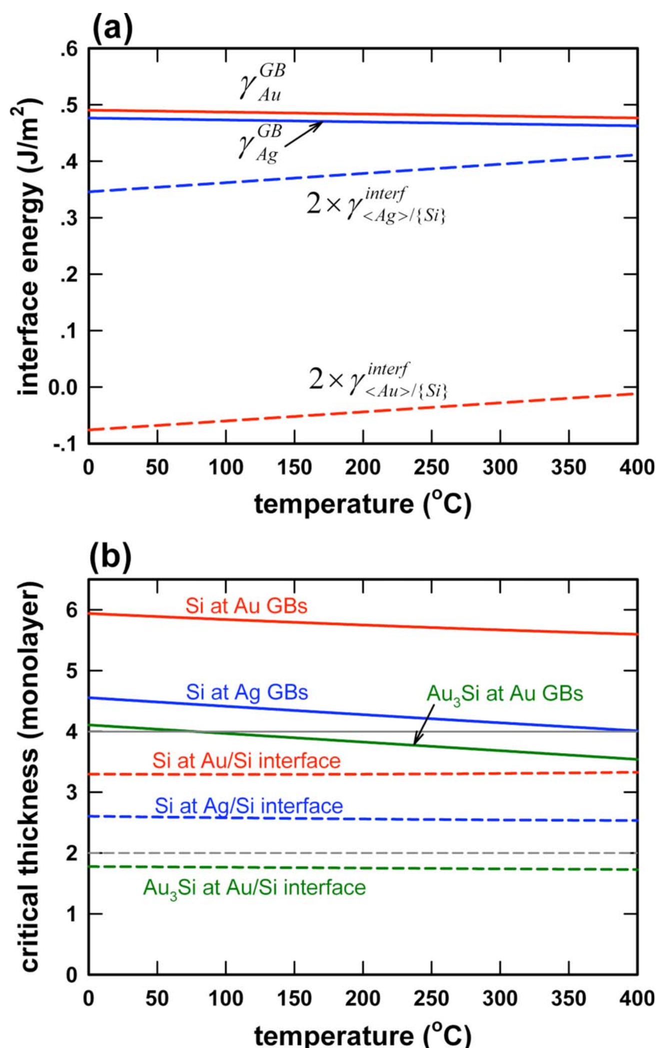

FIG. 8. (Color online) (a) Energetics of Ag and Au grain boundary wetting by a-Si. It follows that a-Si can wet both Ag GBs and Au GBs. (b) Energetics of the nucleation of crystalline Si at Ag and Au GBs and at Ag/a-Si and Au/a-Si interfaces. It follows that c-Si can nucleate at the Ag GBs at (above) ~400 °C. For the Au/a-Si system, it follows that c-Si cannot nucleate directly at Au GBs and at the Au/a-Si interface. MIC in Au/a-Si is, however, mediated by the formation of metastable Au_3Si nucleated at Au GBs (see text).

GBs and at the Au/a-Si interface were performed here using the thermodynamic model presented in this paper.[53] The results of the calculation are also shown in Fig. 8(b). The critical thickness of a-Si at Au GBs to form Au_3Si is close to 4 ML at a low temperature of 80 °C (and is smaller at higher temperatures), which explains the formation of Au_3Si at Au GBs in the range of 100–200 °C.[14,25] At the Au/a-Si interface, the critical thickness is ~1.8 ML (<2 ML), indicating that Au_3Si can also nucleate at the Au/a-Si interface. Recognizing the very large positive driving force for Si atoms diffusing into the Au GBs [see Fig. 8(a)] and also the higher mobility and supply of *Au atoms* at Au GBs,[25] it can be conceived that the formation of Au_3Si will be much more pronounced at Au GBs than at the Au/a-Si interface, which is consistent with experimental observations.[25]

The above discussed calculations and corresponding experimental observations demonstrate the decisive role of interface thermodynamics on phase transformations occurring in small-size systems. The model is capable of predicting, from an energetic point of view, if a certain phase can be formed at a certain location in the microstructure considered.

V. CONCLUSIONS

MIC in immiscible alloy systems at low temperatures can be understood on a thermodynamic, rather than kinetic, basis. Interface thermodynamics is shown to play a decisive role for various kinds of reported MIC behaviors.

For the Al/Si system, the calculations show, in agreement with the experiments, that MIC is the result of the following processes: (i) Al GB wetting, (ii) Al GB nucleation of c-Si, (iii) further wetting of ⟨Al⟩/⟨Si⟩ boundaries by a-Si, parallel to the original Al GBs, and (iv) subsequent lateral c-Si grain growth. The formation of new c-Si nuclei is impossible at the ⟨Al⟩/{Si} and ⟨Al⟩/⟨Si⟩ interfaces at low temperatures.

For the Al/Ge system, the calculations show, in agreement with the experiments, that c-Ge is capable to nucleate both at the Al GBs and at the ⟨Al⟩/{Ge} interface. The interface-mediated crystallization of a-Ge and the GB-mediated (lateral) crystallization of a-Ge occur simultaneously in the Al/Ge layer system.

The thermodynamic model proposed is applicable to evaluate the MIC behaviors in immiscible layer systems, in general, as also shown by its application to the Au/a-Si and Ag/a-Si systems for which experimental observations have been reported previously in the literature.

ACKNOWLEDGMENTS

The authors thank B. Siegle for the assistance with AES and SEM analyses, G. Maier and U. Welzel for the assistance with the *in situ* XRD measurements, and F. Sommer for a helpful discussion.

*j.y.wang@mf.mpg.de

[1] J. M. Howe, *Interfaces in Materials* (Wiley, New York, 1997).
[2] A. P. Sutton and R. W. Balluffi, *Interfaces in Crystalline Materials* (Clarendon, Oxford, 1995).
[3] K. R. Coffey and K. Barmak, Acta Metall. Mater. **42**, 2905 (1994).
[4] K. R. Coffey and K. Barmak, Mater. Res. Soc. Symp. Proc. **343**, 193 (1994).
[5] R. Benedictus, A. Böttger, and E. J. Mittemeijer, Phys. Rev. B **54**, 9109 (1996).
[6] B. X. Liu, W. S. Lai, and Z. J. Zhang, Adv. Phys. **50**, 367 (2001).
[7] L. Zhang, Z. H. Jin, L. H. Zhang, M. L. Sui, and K. Lu, Phys.

Rev. Lett. **85**, 1484 (2000).
[8] L. Zhang, L. H. Zhang, M. L. Sui, J. Tan, and K. Lu, Acta Mater. **54**, 3553 (2006).
[9] E. Pereiro-López, W. Ludwig, D. Bellet, P. Cloetens, and C. Lemaignan, Phys. Rev. Lett. **95**, 215501 (2005).
[10] G. A. López, E. J. Mittemeijer, and B. B. Straumal, Acta Mater. **52**, 4537 (2004).
[11] W. Lojkowski and H. J. Fecht, Prog. Mater. Sci. **45**, 339 (2000).
[12] A. M. Alsayed, M. F. Islam, J. Zhang, P. J. Collings, and A. G. Yodh, Science **309**, 1207 (2005).
[13] T. J. Konno and R. Sinclair, Philos. Mag. B **66**, 749 (1992).
[14] T. J. Konno and R. Sinclair, Mater. Sci. Eng., A **179**, 426 (1994).
[15] Li Bo-quan, Zheng Bin, Zhang Shu-yuan, and Wu Zi-qin, Phys. Rev. B **47**, 3638 (1993).
[16] O. Nast and A. J. Hartmann, J. Appl. Phys. **88**, 716 (2000).
[17] O. Nast and S. R. Wenham, J. Appl. Phys. **88**, 124 (2000).
[18] Y. H. Zhao, J. Y. Wang, and E. J. Mittemeijer, Appl. Phys. A: Mater. Sci. Process. **79**, 681 (2004).
[19] D. He, J. Y. Wang, and E. J. Mittemeijer, J. Appl. Phys. **97**, 093524 (2005).
[20] D. He, J. Y. Wang, and E. J. Mittemeijer, Appl. Phys. A: Mater. Sci. Process. **80**, 501 (2005).
[21] J. Y. Wang, D. He, Y. H. Zhao, and E. J. Mittemeijer, Appl. Phys. Lett. **88**, 061910 (2006).
[22] F. Katsuki, K. Hanafusa, M. Yonemura, T. Koyama, and M. Doi, J. Appl. Phys. **89**, 4643 (2001).
[23] Z. M. Wang, J. Y. Wang, L. P. H. Jeurgens, and E. J. Mittemeijer, Scr. Mater. **55**, 987 (2006).
[24] Hou Jian-guo and Wu Zi-qin, Phys. Rev. B **42**, 3271 (1990).
[25] M. Seibt, S. Buschbaum, U. Gnauert, W. Schröter, and D. Oelgeschläger, Phys. Rev. Lett. **80**, 774 (1998).
[26] J. Jang, J. Y. Oh, S. K. Kim, Y. J. Choi, S. Y. Yoon, and C. O. Kim, Nature (London) **395**, 481 (1998).
[27] E. A. Guliants and W. A. Anderson, J. Appl. Phys. **89**, 4648 (2001).
[28] A. Hiraki, Surf. Sci. Rep. **3**, 357 (1984).
[29] U. Gösele and K. N. Tu, J. Appl. Phys. **53**, 3252 (1982).
[30] F. R. de Boer, R. Boom, W. C. M. Mattens, A. R. Miedema, and A. K. Niessen, *Cohesion in Metals: Tansition Metal Alloys* (North-Holland, Amsterdam, 1988).
[31] F. Sommer, R. N. Singh, and E. J. Mittemeijer, J. Alloys Compd. (to be published).
[32] L. P. H. Jeurgens, W. G. Sloof, F. D. Tichelaar, and E. J. Mittemeijer, Phys. Rev. B **62**, 4707 (2000).
[33] F. Reichel, L. P. H. Jeurgens, and E. J. Mittemeijer, Phys. Rev. B **74**, 144103 (2006).
[34] M. Wohlschlögel, U. Welzel, G. Maier, and E. J. Mittemeijer, J. Appl. Crystallogr. **39**, 194 (2006).
[35] J. Y. Wang and E. J. Mittemeijer, J. Mater. Res. **19**, 3389 (2004).
[36] Z. M. Wang, J. Y. Wang, L. P. H. Jeurgens, and E. J. Mittemeijer, Surf. Interface Anal. (to be published).
[37] H. J. Wen, M. Dähne-Prietsch, A. Bauer, M. T. Cuberes, I. Manke, and G. Kaindl, J. Vac. Sci. Technol. A **13**, 2399 (1995).
[38] J. C. Slater, J. Chem. Phys. **41**, 3199 (1964).
[39] E. P. Donovan, F. Spaepen, D. Turnbull, J. M. Poate, and D. C. Jacobson, J. Appl. Phys. **57**, 1795 (1985).
[40] Considered here as configurationally frozen liquid below the glass transition temperature.
[41] *CRC Handbook of Chemistry and Physics*, 85th ed. (CRC, Boca Raton, FL, 2004).
[42] H. Wawra, Z. Metallkd. **66**, 395 (1975).
[43] T. Iida and R. I. L. Guthrie, *The Physical Properties of Liquid Metals* (Clarendon, Oxford, 1988).
[44] A. A. Stekolnikov and F. Bechstedt, Phys. Rev. B **72**, 125326 (2005).
[45] S. Hara, S. Izumin, T. Kumagai, and S. Sakai, Surf. Sci. **585**, 17 (2005).
[46] I. Galanakis, N. Papanikolaou, and P. H. Dederichs, Surf. Sci. **511**, 1 (2002).
[47] A. T. Dinsdale, CALPHAD: Comput. Coupling Phase Diagrams Thermochem. **15**, 317 (1991).
[48] J. Gröbner, H. L. Lukas, and F. Aldinger, CALPHAD: Comput. Coupling Phase Diagrams Thermochem. **20**, 247 (1996).
[49] L. H. Allen, J. R. Phillips, D. Theodore, C. B. Carter, R. Soave, J. W. Mayer, and G. Ottaviani, Phys. Rev. B **41**, 8203 (1990).
[50] C. V. Thompson, J. Appl. Phys. **58**, 763 (1985).
[51] P. Y. Chevalier, Thermochim. Acta **130**, 33 (1988).
[52] F. G. Meng, H. S. Liu, L. B. Liu, and Z. P. Jin, J. Alloys Compd. **431**, 292 (2007).
[53] The Gibbs energy of formation of Au_3Si (relative to c-Au and a-Si) was taken as -1.6 kJ/mol (Ref. 25). The energy of the $\langle Au_3Si\rangle/\langle Au\rangle$ small-angle boundary (see Ref. 25) was assessed as 1/2 of the large-angle $\langle Au\rangle$ GB energy. The energy of the $\langle Au_3Si\rangle/\{Si\}$ interface was estimated to be the same as that of the $\langle Au\rangle/\{Si\}$ interface.